PUP Journal of Science and Technology (PUPJST)
Volume 17 (2024), (pp. 45-57)

Original Article

Effect of Groin Field Installation in the Shoreline in Agoo, La Union, Philippines

***Arianna Bianca E. Brosas*[1,*], *John Paul L. Santos*[1], *Rogelio G. Dizon*[1], *Rhenish C. Simon*[2]**

[1]*Department of Physical Sciences, College of Science, Polytechnic University of the Philippines, Sta. Mesa, Manila, 1016, Philippines*
[2]*Physics Department, College of Science, De La Salle University, Taft Avenue, Manila, 1004, Philippines*

corresponding email: ariannabrosas11@gmail.com
Received:03 Nov 2023; Accepted 10 Dec 2023; Available online: 08 October 2024

Abstract: Shoreline accretion and erosion are heightened by rising sea levels and powerful storm waves, posing increasing challenges for coastal communities. In response, groin fields—specialized structures built perpendicular to the shore to trap sand—have been implemented. To ensure effective coastal management, ongoing monitoring of these structures is essential. Satellite images from Google Earth were utilized to investigate the groin field's impact on the study area. This study proposes a technique for shoreline position detection and extraction from satellite images through threshold segmentation, edge detection, and automatic curve selection. The processed images provided shoreline positions used to calculate the change in shoreline width before and after the groin field construction. The influence of a groin field on shoreline change is investigated in the coastal zone of Agoo, La Union. Larson's shore model is fitted to the detected shoreline positions utilizing the TikTak global optimization algorithm and the Broyden-Fletcher-Goldfarb-Shanno (BFGS) algorithm. This process determines the optimal shore diffusivity and breaking wave angle for each year that best represents the shoreline position. In regions of the groin field with greater sand transport, higher shore diffusivity values and smaller breaking wave angles are observed. This research can be utilized for preliminary investigations of coastal areas with groin-like structures. Studying the interaction between the groin field and the shoreline provided valuable data for researchers to consider. This information can be used to assist in forming strategies for optimizing groin placement and understanding potential shoreline alterations following their installation.

Keywords: *Groin field impact assessment, Remote sensing, Coastal erosion, Optimization algorithms*

1. INTRODUCTION

As an archipelago, the Philippines has most of its population in coastal areas. Beneficial resources for food production, labor, and tourism can be obtained from these regions (Department of Environment and Natural Resources, 2001). However, this proximity to the coast comes with inherent risks. Driven by factors like rising sea levels and coastal erosion, the usable land area near the shore is constantly shrinking (Leatherman et al., 2000). This

phenomenon threatens the safety and viability of coastal communities and infrastructure. Effective coastal management strategies are necessary to mitigate these threats (Rangel-Buitrago et al., 2020). One approach involves the construction of coastal protective structures, such as breakwaters and groin fields.

The municipality of Agoo, La Union, identified by Climate Central (2022) as highly vulnerable to sea level rise, exemplifies the challenges faced by coastal communities. Home to a population of 66,028 (Philippine Statistics Authority, 2020), Agoo has implemented a groin field along its shoreline as a defense mechanism against coastal flooding. Groins, typically constructed perpendicular to the coast, trap sediment, and aim to stabilize the shoreline. However, research suggests that these structures can also have unintended consequences (Balaji et al., 2017). Therefore, close monitoring of the groin field and its impact on the surrounding environment is crucial to ensure it effectively achieves its intended purpose.

Vaidya et al. (2015) highlighted the importance of considering factors like initial shoreline conditions and sediment transport when designing groins. Their study explored how groin length, number, and spacing affect shoreline changes through simulations. Research by Lim et al. (2021) demonstrates the trade-offs associated with groins. While they can halt shoreline recession, they may disrupt natural sediment transport patterns, leading to erosion in other areas. Their study employed satellite images to assess how groins and other structures like ports affect sediment transport. Their findings suggest that groins can be effective in preventing shoreline retreat but require sand nourishment and proper length considerations. Uda et al. (2021) investigated sand spit elongation near groins on the Cabaruan, La Union shoreline using satellite images. Their observations revealed that sediments naturally move southward from Agoo and Cabaruan, causing the shoreline in Narvacan to be thinner. This highlights the groin's role in interrupting natural sediment transport processes.

Informed by prior studies on the use of satellite images to analyze the impact of coastal structures like groin fields, a deeper investigation is needed. These images, readily available from open-source platforms like Google Earth, offer a valuable alternative to traditional ground monitoring methods. Satellite images allow researchers to observe the dynamic behavior of vast coastlines over extended periods, facilitating the measurement of shoreline changes (Chenthamilselvan et al., 2014).

Groin fields can disrupt the natural transport of sediment along the shoreline. This disruption can create the illusion of an expanding shoreline due to the accumulation of sediment on the updrift side (the side facing the incoming waves). Sediment motion can result in the elimination or addition of volumes of sand. The Coastal Engineering Manual (2002) defines erosion as landward shoreline movement and accretion as seaward movement. While groins may provide localized protection, they can also starve the downdrift side (opposite the updrift side) of sediment, leading to erosion. Therefore, it is crucial to study how the specific conditions of an area, including the implemented groin and wave direction, influence shoreline changes.

As the wave approaches the shoreline at an angle, the sediment moves along the shoreline in the direction of wave propagation. Calculated accretion and erosion can reveal some of the mechanisms behind the sediment movement and ocean wave properties in the coastal area (Bidorn & Rukvichai, 2018). Larson et al. (1987), provided a mathematical model for the interaction of the ocean wave and groin field, where shore diffusivity and breaking wave angle are some of the parameters used to describe the change in shoreline through time. Shore diffusivity describes how much sand is transported alongshore through time. The other parameter refers to the angle between the breaking wave crests approaching the shore and the groin field. By understanding these parameters and their impact on the resulting shoreline, coastal management strategies can be improved. In this study, an assessment of shoreline response to the constructed groin field in Agoo, La Union is undertaken by using satellite images of the coastal zone.

Figure 1. The area of interest is located at latitude 16° 21′ N and longitude 120° 20′ E. The study area has a length of 447.11 m and a width of 210.44 m.

2. METHODOLOGY

2.1 Collection and Digitization of Satellite Images

Satellite images from 2013 to 2022 of the study area in Agoo, La Union, were obtained from Google Earth. In Table 1, the details of the acquired satellite images are shown. Only satellite images with clear conditions are included in the shoreline change calculations. Throughout all of the acquisition dates, the image alignment in relation to the nearby coastal structures was confirmed. The study area's measurements were chosen in order to observe how the groin field interacts with the shoreline, which was done by giving priority to the shoreline sections where the groin field is located. High-resolution images from CNES, Airbus, and Maxar were utilized in the procedures. These applications were also used in numerous studies on land mapping and monitoring, as shown by Gibbs et al. (2020) and Clark et al. (2022). Figure 2 shows some of the outputs for the digitization of the collected images.

Table 1. Details of satellite images from Google Earth.

Year	Months	No.	Condition
2013	Oct	1	Dark tone
2014	Feb	1	Clear
2015	Feb, June	2	Clear, blurry
2016	Feb, Mar, Apr, Nov, Dec	5	Clear, cloudy, blurry, clear, clear
2017	Apr, May, Nov, Dec	4	Clear, dark tone, clear, clear
2018	Feb	1	Clear
2019	Feb, Mar, Oct, Dec	4	Clear
2020	Oct, Nov	2	Clear, dark tone
2021	Jan, Mar, Apr	3	Clear
2022	Mar, Apr, May	3	Clear

The acquired satellite images were uniformly cropped to highlight the coverage of the study area. Threshold segmentation was then applied to the cropped image in Figure 2a to obtain a binary image. Image thresholding involves classifying pixel values within the image

(Gonzales & Woods, 2006). As illustrated in Figure 2b, the resulting image has pixel values of 0 for black and 255 for white. Edge detection was subsequently employed on the image in Figure 2c to identify the boundary between land and ocean areas, which corresponds to the shoreline position. Finally, the shoreline position was extracted using WebPlotDigitizer, as depicted in Figure 2d.

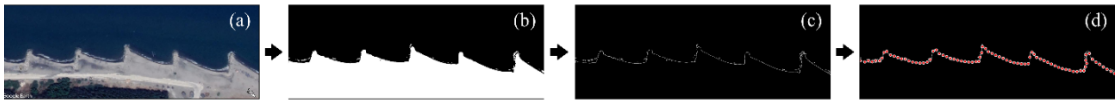

Figure 2. Processing of (a) satellite image from April 2021; (b) threshold segmentation; (c) edge detection; (d) extraction of shoreline position.

2.2 Calculation of the Shoreline Change

The shoreline positions from 2013 to 2016 were classified as the pre-construction phase, while the subsequent years, from 2017 to 2022, were designated as the post-construction phase. As seen in Figure 3a, 20 transect points were identified and were used to provide an estimation of how much of the shoreline has changed from its initial state to its succeeding forms. Transect points located above the initial shoreline (2016) in Figure 3a, such as points 7 to 20, indicate accretion. Conversely, points positioned below the initial shoreline, like points 1 to 6, signify erosion. The method used in the observation of shoreline change to track the evolution of areas of interest was adapted from Harley (2019) and Gibbs (2020). The tide level in the study area was considered in the computation for accretion and erosion from the extracted shoreline positions. There is an online database where the estimated values for the tide level in La Union were obtained ("Tide Times and Charts for Lingayen Gulf," 2022). Figure 3b provides the partition of the regions within the groin field from a to f. Each area is bounded by a groin as a clear division between the coverage of the regions. Images of the study area are presented, showing the pre-construction and post-construction phases of the groin field.

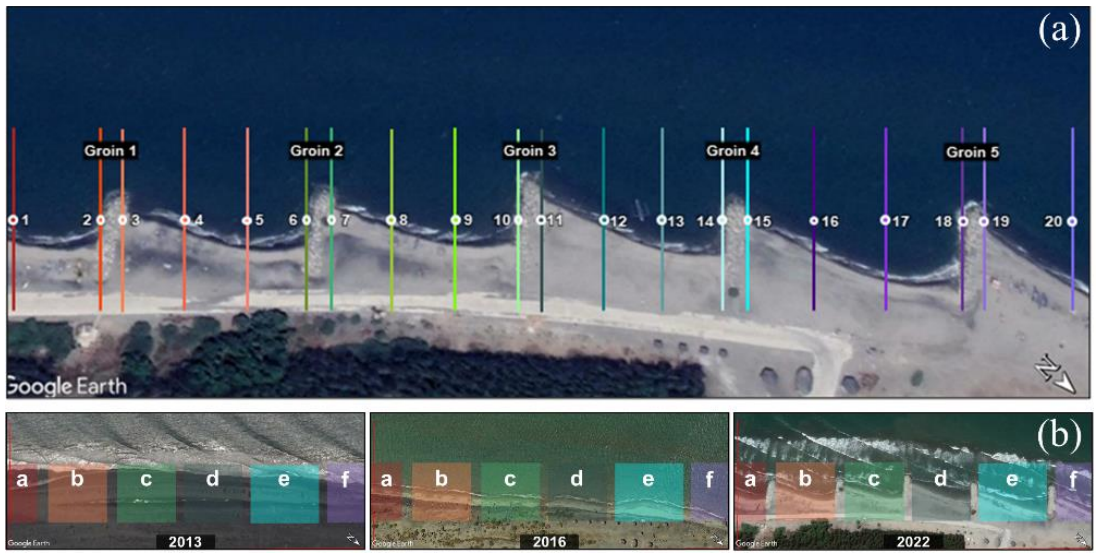

Figure 3. The portions of the study area with their corresponding labels to aid the discussion of the methods and results: (a) transect points; (b) regions within the groin field.

The extracted shoreline positions were then used to calculate several parameters describing the shoreline evolution within the groin field. These parameters are derived from Larson's shore model, which accounts for the impact of groins on shoreline behavior. As demonstrated by previous studies (Baykal, 2006; Unyapoti & Pochai, 2020), Larson's model effectively estimates shoreline evolution. The model adheres to the boundary condition where the shoreline remains parallel to incoming wave crests. Notably, the study area possesses the same source for transported sediments and wave crest direction as assumed by the model. However, a key difference exists. Larson's model assumes the shoreline at $x = 0$ and the groin at $y = 0$, with the shoreline extending from 0 to the positive x direction. In contrast, the area of interest comprises six regions with varying coordinates, as illustrated in Figure 3. To address this discrepancy, parameters x_0 and y_0 were introduced allowing the function to be translated to the appropriate position for each groin (Brosas et al., 2023).

$$y(x,t) = 2\tan\alpha_0 \left\{ \sqrt{\frac{\varepsilon t}{\pi}} \exp\left[\frac{-(x-x_0)^2}{4\varepsilon t}\right] - \frac{x-x_0}{2}\operatorname{erfc}\left(\frac{x-x_0}{2\sqrt{\varepsilon t}}\right)\right\} + y_0. \quad (1)$$

In equation 1 α_0 is the breaking wave angle, ε is the diffusivity parameter (m^2/s), t for time (s), x is the alongshore distance (m), x_0 is the x-offset, y_0 is the y-offset, and erfc is the complementary error function. The parameter x_0 for a groin is set to be the x-position where the groin meets the shoreline, while the parameter y_0 is set to be the average y-position of the 2016 shoreline for a groin (Brosas et al., 2023). Without translating the function, the model only recognizes the study area as a shoreline with only one groin. Contrary to the actual condition of the study area with multiple groins, there are portions of the shore on the left side of the groin. The function describing the shoreline change in these regions is mirrored on the y-axis.

The mean squared error (MSE) loss function is then defined as,

$$L(\alpha_0, \varepsilon) = \frac{1}{n}\sum_{i=1}^{n} |y_i - y(x_i, t)|^2, \quad (2)$$

where (x_i, y_i) is a coordinate of the shoreline for a groin. The loss function is equal to zero when the parameters α_0 and ε make the function $y(x_i, t)$ equal to y_i at time t. To find the best-fit parameters that describe the shoreline for each year, the total loss function was aimed to be minimized by,

$$\min_{\alpha_0,\varepsilon} L_1(\alpha_0 + 90°, \varepsilon_1) + L_2(\alpha_0, \varepsilon_2) + L_3(\alpha_0, \varepsilon_3) + L_4(\alpha_0, \varepsilon_4) + L_5(\alpha_0, \varepsilon_5) + L_6(\alpha_0, \varepsilon_6), \quad (3)$$

where L_i is the loss function for a region, subject to the constraint that the breaking wave angle α_0 is the same for all regions. To satisfy the constraint, the loss for L_1 has an additional $90°$ term because the function for that region is mirrored about the y-axis (Brosas et al., 2023). One value for the breaking wave angle and a total of six values for shore diffusivity are identified for each year. The assumption of having the same breaking wave angle in the study area is based on Larson's shore model. Larson et al. (1987) explained that applying their solution where a change in shoreline occurs due to a groin requires the case to be idealized to a large degree. Which includes the assumption that the beach profile is in equilibrium with average wave conditions.

To reduce the overall loss function, the TikTak global optimization algorithm was utilized. It uses multiple starting parameters to perform local optimization, ultimately considering the outcome with the lowest loss value as the global minimum. The performance of this algorithm is verified by numerous benchmarks, showing its reliability and efficiency (Arnoud et al., 2019). The Broyden-Fletcher-Goldfarb-Shanno (BFGS) algorithm is employed to carry out the local

optimization at each starting point (“Quasi Newton Methods,” 2006). It is an algorithm that non-linear optimization frequently uses.

In Figure 4, Larson's shore model is optimized to determine the values of breaking wave angle and shore diffusivity that minimize the loss function. This optimization is achieved through the TikTak algorithm. The implementation process begins with initialization, where bounds are set for each parameter and a sequence of Sobol's points is generated. Subsequently, the BFGS algorithm, acting as the local optimizer, is applied along with a pre-defined stopping criterion. A local search is then conducted until a local minimum is identified and recorded. Finally, the program returns the parameter vector with the lowest function value as the global minimum. The TikTak and BFGS algorithms were implemented using the Julia programming language, as described by Bezanson et al. (2012).

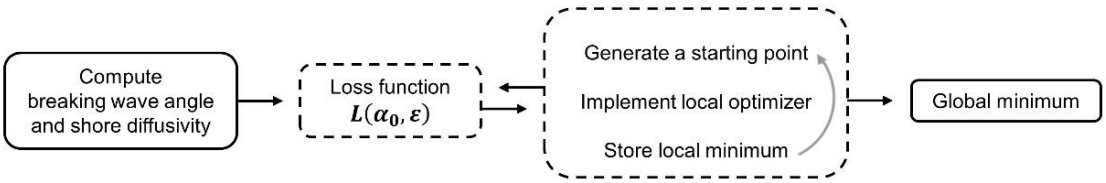

Figure 4. The above figure shows the procedures for optimization. The operations with dashed borderlines were performed multiple times until the best local minimum was returned as an estimation of the global minimum.

3. RESULTS AND DISCUSSION

3.1 Before the Construction of Groin Field (2013-2016)

Figure 5 shows the trend of shoreline change. This phase considers the extracted shoreline for 2013 as the initial shoreline and the plotted points for 2016 as the final shoreline position. Both the initial and final shorelines are depicted as dashed lines with corresponding transect points. The distance measured between these transect points is then visualized in the bar graph within Figure 5. The bar graph clearly reveals a landward movement of the shoreline from 2014 to 2016 compared to its initial positions, indicating an overall receding trend. The portion of the shore on the right side of Figure 5 appears to experience more erosion. This can be attributed to the unimpeded movement of sand from the northern section towards the southern part of the shore during this phase.

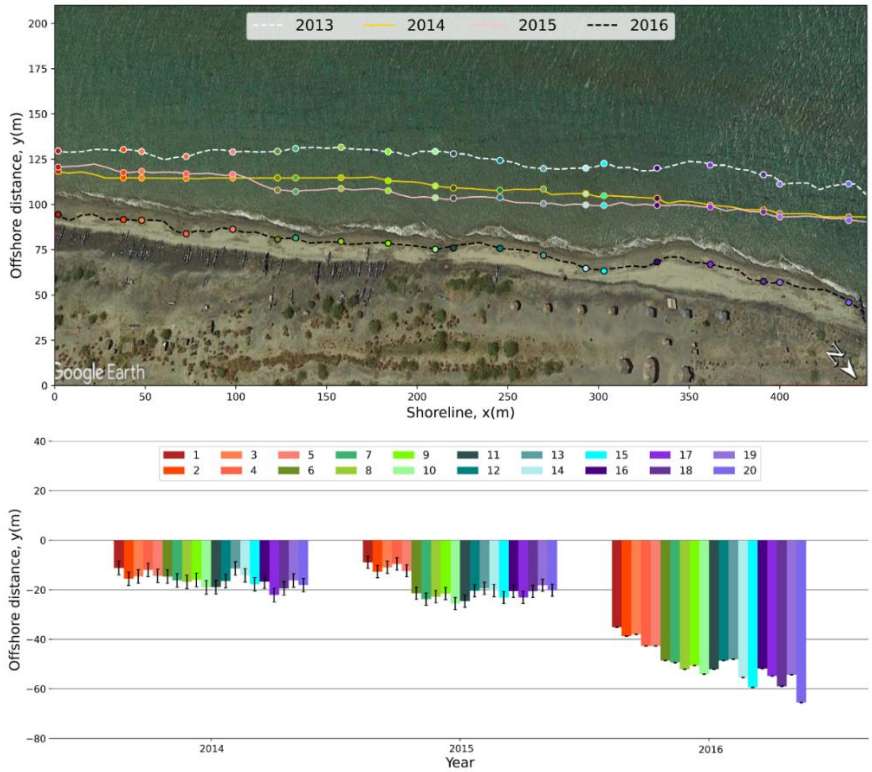

Figure 5. Pre-construction visualization of the extracted shoreline positions.

3.2 After the Construction of Groin Field (2016-2022)

The visualization in Figure 6 shows how the shoreline has changed since the coastal protective structure was built. The plotted data points for 2022 are taken to be the final shoreline, while the extracted shoreline for 2016 is treated as the initial shoreline. Satellite images show that the incident ocean wave originates in the study area's northern region, which corresponds to the right side of Figure 6. In the study area, sediment is transported in the same direction as the incident ocean wave (Splinter et al., 2012). This explains why, on each groin's right side, the shoreline appears to be getting wider. Whereas, on its left side, it appears to be getting narrower. In the upcoming years, it is predicted that this trend will persist. A related study conducted in Cabaruan, La Union, supports this finding (Uda & Serizawa, 2021). Their study area is also part of the Lingayen Gulf, which is located near Agoo, La Union.

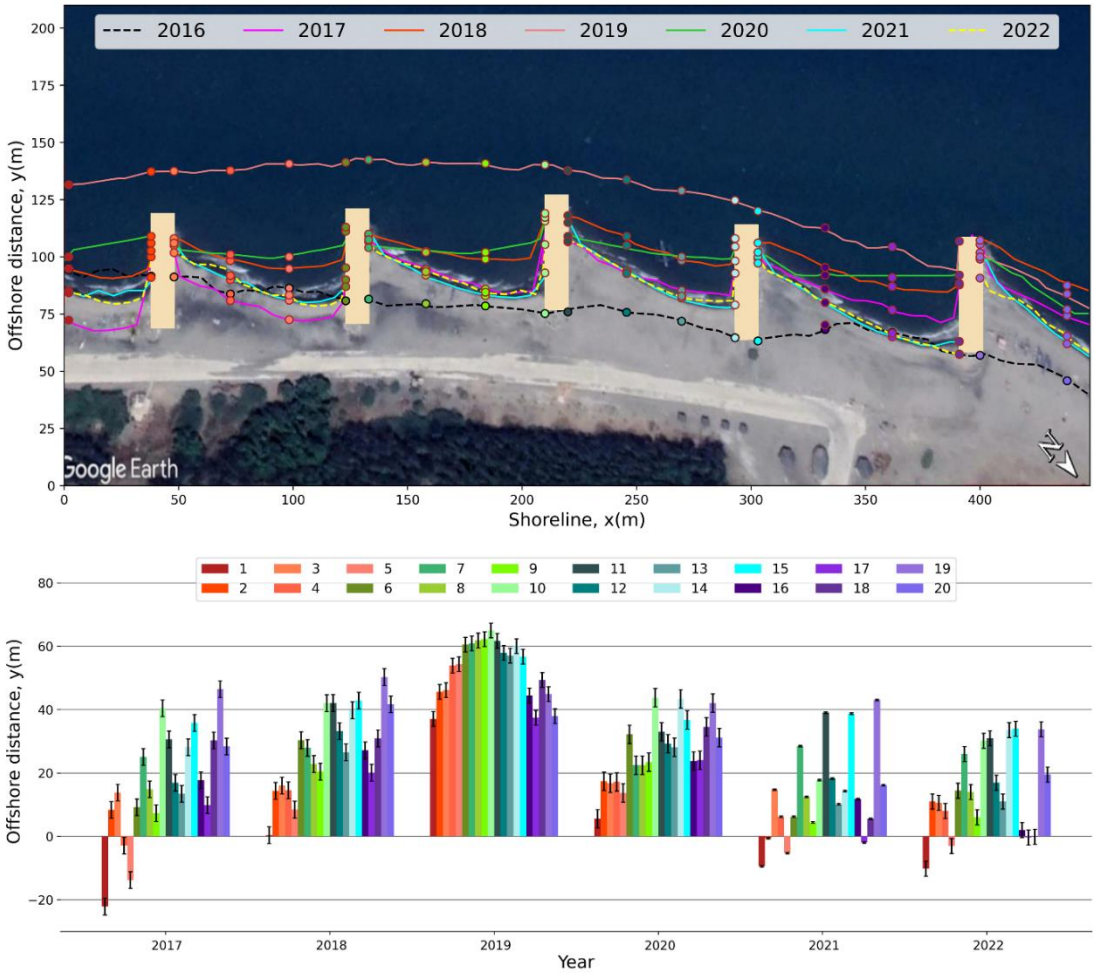

Figure 6. Post-construction visualization of the extracted shoreline positions.

In Figure 6, the first and second groins' downdrift portions of the shoreline are experiencing erosion in 2017, while the rest of the shoreline is experiencing accretion. The groin's updrift portion experiences accretion, while its downdrift portion experiences erosion. This finding is consistent with the descriptions found in other works of literature and research done by Kamphuis (2010), Bidorn and Rukvichai (2018). The width of the shoreline has generally increased from 2018 to 2019. The most significant amount of sand accretion is seen in 2019, as shown in Figure 6, which is still connected to the interrupted sand transport after the groin field is put into place. The detected shoreline positions for 2020 and 2021 exhibited a decrease in width, while the shoreline position in 2022 remains closer to the preceding year. Evidence of erosion is present at transect points 1, 5, 17, and 18 in 2022, with transect point 1 showing the greatest amount of erosion at a 10.17 m decrease in shoreline width. The remaining transect points show accretion, with transect point 19 showing the largest increase in shoreline width at 33.81 m. It is clear that some shoreline features of the study area underwent accretion and erosion. It was observed from the satellite images that sand from the portion of the beach beyond the groin field is transported toward the study area. The groin field is advantageous to the area where it is located, but it may be harmful to the parts of the beach that are not protected because this part of the shoreline is subject to erosion (Brosas & Simon, 2022). Through these observations, the evolution of the shoreline from its position in 2016 to its current state in 2022 can be understood.

3.3 Shore Diffusivity and Breaking Wave Angle

Shore diffusivity, defined as the rate of sediment transport along a shoreline by wave action (Ciccaglione et al., 2022), is impacted by the installation of groin fields. This localized effect alters the diffusivity within the area. Studying shore diffusivity, or sediment spreading, is crucial for understanding how groin fields trap sand and contribute to erosion patterns. A close relationship exists between shore diffusivity and the breaking wave angle, defined as the angle of breaking wave crests relative to the shoreline trend. This association arises due to Larson's shore model, which employs both breaking wave angle and shore diffusivity to characterize shoreline change. Furthermore, studies (Falques, 2003) demonstrate an inverse relationship between diffusivity and the breaking wave angle, with diffusivity decreasing as the wave angle increases.

Larson's shore model was used to determine shore diffusivity and breaking wave angle. A fitted function derived from this model was applied to achieve this. Equation 1, which presents Larson's shore model, utilizes both shore diffusivity and breaking wave angle to describe shoreline change. Given the detected shoreline positions within the study area, optimization algorithms are applied to fit Larson's model to these extracted positions from the satellite images. This fitting process enables the calculation of shore diffusivity and breaking wave angle values. The groin field's spaces are labeled from a to f. The average shore diffusivity for each region of the detected shoreline positions each year is shown in figure 7a. In 2019, the highest shore diffusivity of 7.55×10^{-4} m²/s was calculated. The middle section of the groin field's regions c and d have the highest shore diffusivity. Other shores where a groin field is present also exhibit differences in the distribution of the sediment material observed in the study area (Kim et al., 2013). Figure 6 shows that 2019 is also the year with the largest increase in shoreline width. In the study area, sediment from other parts of the shore is deposited; this is also the case in the study of Dalrino et al. (2021). This is in accordance with the function of the groin field, which is to contain the sand in its area. Figure 7b shows that its breaking wave angle of 9.68° is among the smallest computed values derived from the fitted function. This indicates that the wave's breaking crests are moving horizontally in the direction of the groin's vertical placement. In this particular year of 2019, the current is probably strong, and the transport of sediment is greater than in other years. The shore diffusivities for 2021 and 2022 are clearly the lowest when compared to other years in figure 7a. Their calculated average values are 3.98×10^{-6} m²/s and 4.73×10^{-6} m²/s, respectively. Figure 6 illustrates the decline in shoreline width following its peak in 2019. A decline in the rate of sediment diffusion along the shoreline is indicated by less sand. For 2021 and 2022, the breaking wave angles are 45.95° and 39.26°, respectively. In contrast to 2019, there may be a weaker current and less sediment transport due to the larger angle between the breaking wave crests and the groin.

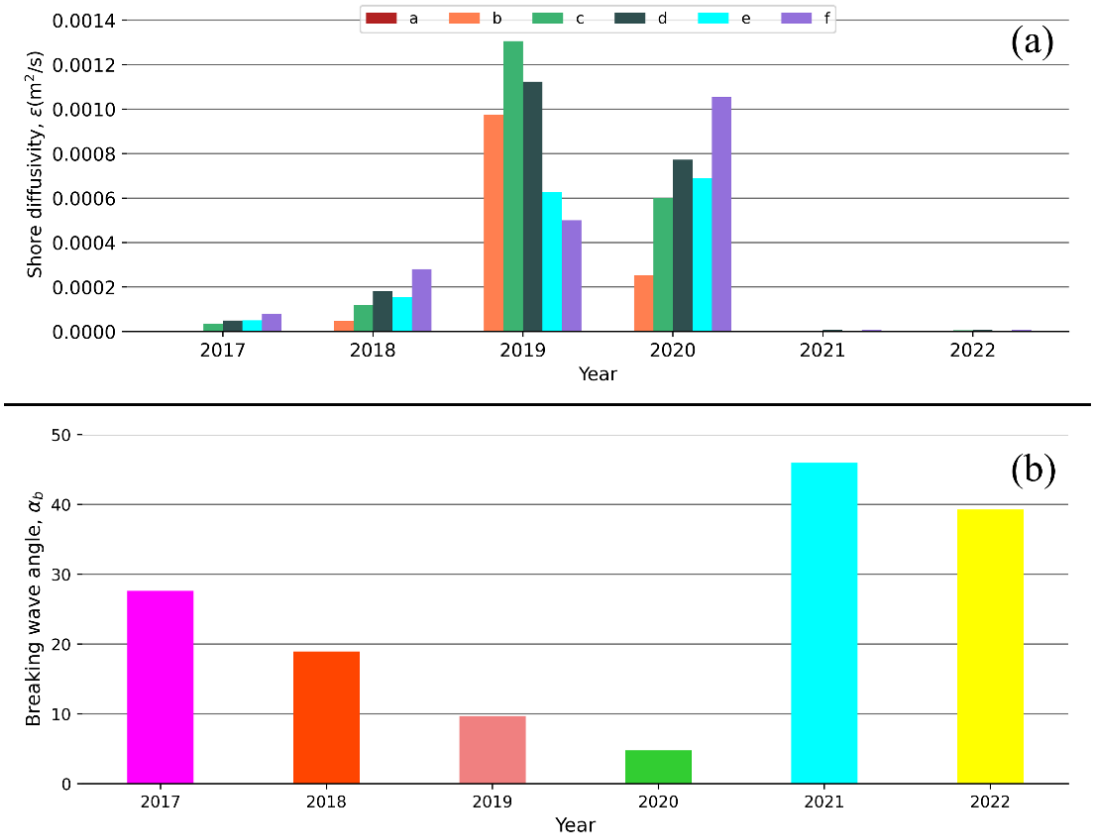

Figure 7. Calculated (a) shore diffusivity and (b) breaking wave angle from the fitted function.

4. CONCLUSIONS

Satellite images of the shoreline in Agoo, La Union, were analyzed to assess its evolution in response to the constructed groin field. Image processing techniques and subsequent application of optimization algorithms, along with Larson's shore model, were used to characterize this response.

An average decrease in shoreline width was recorded from 2014 to 2016 (28.37 m) prior to groin field construction. Following construction, average decreases were calculated from 2017 to 2019 (17.60 m) and 2020 to 2022 (31.56 m), with 2013 serving as the initial shoreline position. Analysis of shore diffusivity revealed an initial increase across all regions following construction. Maximum diffusivity (8.01×10^{-5} m²/s and 2.81×10^{-4} m²/s) was observed in region f during 2017 and 2018, respectively. However, diffusivity decreased in all areas except region f from 2020 onwards. Conversely, the breaking wave angle exhibited a decreasing trend from 2017 to 2020 followed by an increase from 2021 to 2022. Ashton and Giosan (2011) investigated the influence of wave angle on sediment accumulation in a river delta, which exhibits groin-like behavior. Their findings indicate that diffusivity values increase with decreasing wave angles.

Through identification of sand accumulation patterns within each groin field region, portions effective in reducing coastal erosion were distinguished. Additionally, estimations of the parameters influencing these changes were determined. Overall, the presence of groins in the study area impacts the dynamics of the shore.

5. ACKNOWLEDGMENT

The authors would like to acknowledge the support of the Department of Science and Technology – Science Education Institute and the Polytechnic University of the Philippines – Research Institute of Science and Technology in conducting this study. The research funding was provided by these institutions, which facilitated the achievement of the research objectives.

6. REFERENCES

Arnoud, A., Guvenen, F., & Kleineberg, T. (2019). Benchmarking Global Optimizers. *ERN: Econ. & Stat. Methods*.

Ashton, A., & Giosan, L. (2011). Wave-angle control of delta evolution. *Geophys. Res. Lett., 38*(13).

Balaji, R., Sathish, K., & Ankita, M. (2017). Understanding the effects of seawall construction using a combination of analytical modelling and remote sensing techniques: Case study of Fansa, Gujarat, India. *Int. J. Ocean Clim. Syst., 8,* 153-160.

Baykal, C. (2006). Numerical modeling of wave diffraction in one-dimensional shoreline change model. *M.S. - Master of Science, Middle East Technical University*.

Bezanson, J., Karpinski, S., Shah, V., & Edelman, A. (2012). Julia: A fast dynamic language for technical computing. arXiv preprint arXiv:1209.5145.

Bidorn, B., & Rukvichai, C. (2018). Impacts of Coastal Development on the Shoreline Change of the Eastern Gulf of Thailand. *IOP Conf. Ser.: Earth Environ. Sci., 171,* 12007.

Brosas, A.B.E., & Simon, R.C. (2022). Shoreline delineation using Google Earth images: A case study for Agoo, La Union, Philippines. *Proceedings of the Samahang Pisika ng Pilipinas.*

Brosas, A.B.E., Santos, J.P.L., & Simon, R.C. (2023). Characterization of shore response to a groin field using TikTak and BFGS optimization algorithms. *Proceedings of the Samahang Pisika ng Pilipinas.*

Chenthamilselvan, S., Kankara, R., & Rajan, B. (2014). Assessment of shoreline changes along Karnataka coast, India using GIS & remote sensing techniques. *Indian J. Mar. Sci., 43,* 1286-1291.

Ciccaglione, M.C., Calabrese, M., & Buccino, M. (2022). Negative Diffusivity of Shorelines via the Littoral Drift Rose Concept. *Environ. Sci. Proc., 21,* 78.

Clark, A., Moorman, B., Whalen, D., & Vieira, G. (2022). Multiscale Object-Based Classification and Feature Extraction along Arctic Coasts*. Remote Sens., 14*(13).

Coastal Risk Screening Tool: Sea level rise and coastal flood risk maps. (2022). Climate Central Org. https://coastal.climatecentral.org/map.

Dalrino, Herdianto, R., & Silitonga, D. (2021). Study of groin structures effectiveness for against abrasion in Padang Beach*. IOP Conf. Ser.: Earth and Environ. Sci., 708*(1), 012035.

Department of Environment and Natural Resources. (2001). *Philippine Coastal Management Guidebook.* Coastal Resources Management Project of Department of Environment and Natural Resources, Cebu City, Philippines.

Falques, A. (2003). On the diffusivity in coastline dynamics. *Geophys. Res. Lett., 30, 2119.*

Gibbs, A., Jones, B., & Richmond, B. (2020). A GIS compilation of vector shorelines and coastal bluff edge positions, and associated rate-of-change data for Barter Island, Alaska*. U.S.G.S*.

Gonzales, R., & Woods, R. (2006). *Digital Image Processing.* Prentice-Hall, Inc., United States.

Harley, M., & Vos, K. (2019). Shoreline change mapping using crowd-sourced smartphone images*. Coastal Engineering, 150,* 175-189.

Herbich, J.B., & Haney, J.P. (1984). Coastal Erosion. *Beaches and Coastal Geology* (pp. 265-267). Springer.

Kamphuis, W. (2010). *Introduction to Coastal Engineering and Management*. World Scientific Publishing Company.

Kim, I.H., Lee, H., Cho, W.C., & Song, D. (2013). Shoreline changes due to groin construction in Namae and Sodol Beaches, South Korea*. J. Coast. Res., 65,* 2131-2136.

Larson, M., Hanson, H., & Kraus, N. (1987). *Analytical solutions of the one-line model of shoreline change*. U.S. Army Engineer Waterways Experiment Station.

Leatherman, S., Zhang, K., & Douglas, B. (2000), Sea level rise shown to drive coastal erosion. *Eos Trans. AGU, 81*(6), 55–57.

Lim, C., Lee, J., & Lee, J. (2021). Simulation of Bay-Shaped Shorelines after the Construction of Large-Scale Structures by Using a Parabolic Bay Shape Equation*. J. Mar. Sci., 9*(1).

Mohanty, P., Patra, S., Bramha, S., Seth, B., Pradhan, U., Behera, B., Mishra, P., & Panda, U. (2012). Impact of Groins on Beach Morphology: A Case Study near Gopalpur Port, East Coast of India*. Journal of Coastal Research, 28*(1), 132-142.

Philippine Statistics Authority. (2020). *Total Population by Province, City, Municipality and Barangay.* https://psa.gov.ph/content/highlights-region-i-ilocos-region-population-2020-census-population-and-housing-2020-cph.

Rangel-Buitrago, N., Neal, W., & de Jonge, V. (2020). Risk assessment as tool for coastal erosion management. *Ocean & Coastal Management, 186.*

Quasi Newton Methods. (2006). Numerical Optimization. Springer, New York.

Splinter, K., Davidson, M., Golshani, A., & Tomlinson, R. (2012). Climate controls on longshore sediment transport*. Cont. Shelf Res., 48.*

Tide Times and Charts for Lingayen Gulf. (2022). Tides Table. http://tides4fishing.com/ph/philippines/santo-tomas-lingayen-gulf.

Uda, T., & Serizawa, M. (2021). Elongation of a Sand Spit Offshore of Groins Due to High-Angle Wave Instability*. Global Media Journal, 19*(7).

Unyapoti, & Nopparat Pochai (2020). A One-Dimensional Mathematical Model of Long-Term Shoreline Evolution with Groin System using an Unconditionally Stable Explicit Finite Difference Method*. International Journal of Simulation: Systems, Science and Technology*.

US Army Corps of Engineers. (2002). *Coastal Engineering Manual.* West Virginia, United States.

Vaidya, A. M., Kori, S. K., & Kudale, M. D. (2015). Shoreline Response to Coastal Structures. *Aquatic Procedia*, *4*, 333–340.